Seeding behavior of TiO_2 particles in supersonic flows

JIALE SONG*, ZHIMI ZHOU, CHANCHAN LI, DEJIN CHENG
College of Materials Science and Engineering, Chang'an University, Xi'an 710064, China

In this work, the Particle Image Velocimetry (PIV) technique was applied to study the compressible supersonic flow regimes into the Multi-Mach number High-speed (MMH) wind tunnel. To generate sufficient light scattering and flow across shock waves, tracer particles and seeding technique were used, and the scattering and tracking of particles were investigated using the experimental observations and theoretical analysis. It was determined that the actual particle diameter should be around 200nm to grantee an adequate aerodynamic response to velocity gradients in the flow. It was further shown from the PIV measurements over a sharp cone that the uniformity of seeding particles dispersion was very important for the operations of the seeding facility. The present study indicated that PIV technique could be an efficient method for monitoring the flow field of shock wave and subsonic flow regimes.

(Received September 05, 2013; accepted July 10, 2014)

Keywords: Seeding, TiO_2, Supersonic flow

1. Introduction

Particle image velocimetry (PIV) has played an important role in modern flowfield diagnostics during the past decade [1]. In PIV, the velocity of particles suspended in the flow was measured as the velocity of flow. In this respect, seeding particles can be considered to be the actual velocity probes, and seeding considerations are very important in PIV. Recently the technique has been extended to measurements of high speed flows [2,3]. Problems arise in the behavior of tracer particles in association with large velocity gradients supersonic flows that particles cannot accelerate or decelerate as rapidly as the flow, especially in the shock wave flow regime.

The application of PIV in high-speed flows pioneered by Moraitis [4] and Kompenhans [5] that the seeding particle tracing accuracy was paid great attention to. A systematic analysis of the scattering and geometrical seeding properties and the application of seeding PIV materials in gaseous media was provided by Melling [6]. The pioneering application of PIV to the hypersonic regime in shock tubes of TUDelft at free stream gas velocity in excess of 1,000m/s showed that the particle relaxation time becomes a crucial factor for the velocity measurement precision [7]. Recently a PIV experimental study to the evaluation of the particle response time across a stationary shock wave was carried out by D. Ragni etal. [8] and the results showed that particles with dynamic size below 100nm yield the shortest time response generally less than 2μs that seems to be most crucial of the problem. In these years, Chinese domestic scholars have carried out many meaningful researches on applications of PIV measurements in supersonic flows. Yi and Zhao [9,10] have successfully exploited NPLS technique and achieved high time and spatial resolution results on supersonic turbulent mixing layer and supersonic free-vortex aerodynamic window; Dai et.al. [11] have carried out experimental study of supersonic jet flow using DPIV and obtained good results. Despite much progress has been made, the analysis of the characteristics of tracer particles was not enough comprehensive and detailed, the seeding technique need to be more in-depth studies.

The very fundamental step in the PIV is selection of a proper particle material and size. The size of the particles should scatter sufficient light for image acquisition and follow the flow faithfully. Most of the researchers have considered that a compromise between reducing the particle size to improve flow tracking and increasing the particle size to improve light scattering. But if the Rayleigh Scattering is considered, small particles approach to molecules may scatter enough light in term of scattering theory and the perfect particle size is around 200nm when the wavelength of the light is 532nm followed the scattering analysis. Otherwise seeding particles into the facility should meet the demands that the particles do not agglomerate too much and get disturbed evenly in the tube.

In the following sections, this paper will consider the specification for PIV seeding particles with respect to light scattering characteristics, the tracking capability and the seeding technique. The PIV measurements over a sharp cone at Ma=4.0 were investigated in comparison with the CFD and schlieren visualization and the results showed that PIV would be considered as an efficient method for measuring the shock wave flowfield as for subsonic flow regimes.

2. Experimental apparatus

2.1 Flow facility

All the PIV measurements were conducted in SJTU MMH(Multi-Mach number High-speed) wind tunnel shown in Fig. 1. This facility is a blow-down type tunnel

designed for Ma=2.5, 3.0, 4.0, 5.0, 6.0, 7.0 and the tests mentioned in this paper were mostly conducted at Ma=4.0 with the free stream velocity measured to be 780m/s(u=780m/s). The operative range of the unit Reynolds number is 2.11×10^6 /m. The nozzle has Φ200mm diameter and the time with steady flow condition is more than 10 seconds. The flow inside the test chamber is optically accessible through three windows with Φ180mm.

Fig. 1. Site of the MMH Wind Tunnel.

2.2 PIV system

The two-components PIV system is composed of a double pulsed Nd:YAG laser at a wavelength of 532nm with a maximum energy of 500mJ and a duration of 6-8ns. The illuminated area is 90mm×65mm. An IPX-11M camera with 4000pix×2672pix(with a pixel size of $9\ \mu m \times \mu m$)is used and equipped with 105 mm SIGMA objective at f# =2.8. The cross-correlation of the PIV recording is performed with MicroVec2. The interrogation windows of sizes 32pix×32 pix is used with an overlap factor of 50%. Fig. 2 shows the schematic of the PIV setup. In section 5 of this paper, the seeding technique and particles generator are introduced in detail.

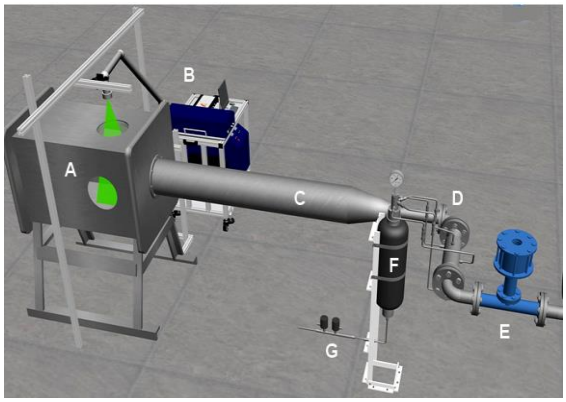

Fig. 2. Schematic of the PIV setup A: Test chamber; B: PIV system; C: Setting chamber; D: Pipes with particles passing by; E: High temperature fast pneumatic valve; F: Particles generator; G: Electromagnetic valve.

2.3 Test models

There are two models used in the tests. The oblique shock wave for measurement of particles response is induced by a ramp configuration with 28 mm long and a deflection angle $\theta = 20°$. Another model for PIV verification of flow investigation is a sharp cone configuration with 65mm in length, 17.5mm in diameter and $\theta = 15°$ in semi-apex angle. The 3D sketches and installed positions of two models are shown in Fig. 3.

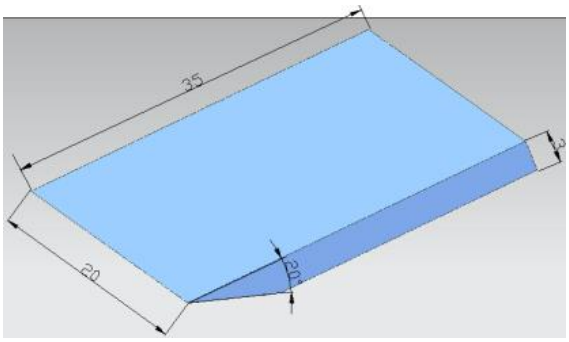

(a)

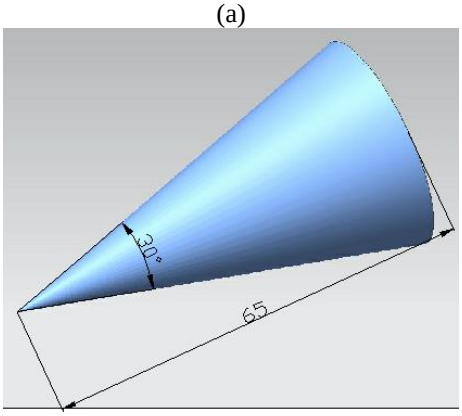

(b)

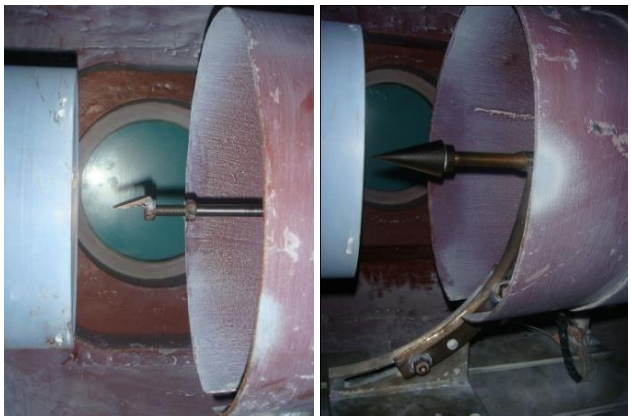

(c) *(d)*

Fig. 3. The 3D sketches and installed positions of test models. (a) ramp;(b) sharp cone;(c) site of ramp; and (d) site of sharp cone.

2.4 Schlieren visualization

Schlieren visualization is used as a complementary flow diagnostic tool. The schlieren system is shown in Fig.4 .Short exposure flow images are obtained by a CCD camera with 1000Hz sample rate and 60 μs exposure time. The resolution is 1024pix×1024pix and the flowfield of visualization is Φ180mm.

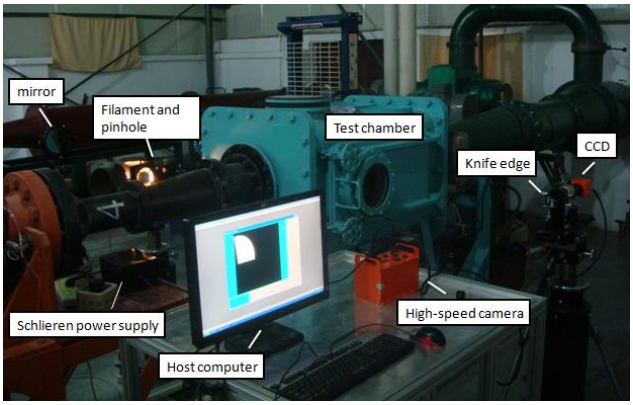

Fig. 4. Site of the schlieren system in MMH wind tunnel.

2.5 Seeding particles

In order to choose proper particle size, four specifications of Titanium dioxide(TiO_2) particles with different diameters are selected as seeding particles, respectively D10,D30,D90 and D30b, where D30b is a different type (produced by another factory)from the others. The qualitative inspection of four specifications of particles using an electron microscope (SEM-imaging) to reveal the agglomeration effects are shown in Fig. 5. Actual particles diameters can be estimated around 200nm, 200nm, 300nm and 200nm from Fig. 5 and listed in Table1. (D10 was easier to agglomerate learned from the factory). The actual size of these four specifications of particles will be further determined and identified through the oblique shock wave response analysis in following section 4.

Table 1. Seeding particles physical properties.

Seeding identification	Nominal size [nm]	Estimated actual size [nm]	Bulk density [kg/m^3]
D10	10	~200	4230
D30	30	~200	4230
D90	90	~300	4230
D30b	30	~200	4230

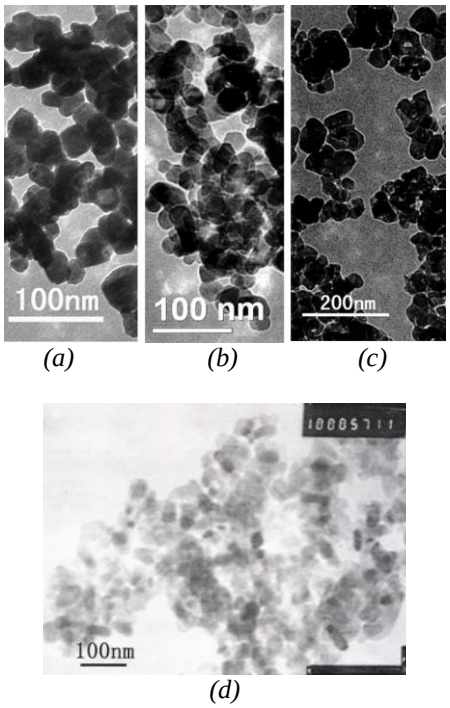

(a) (b) (c)

(d)

Fig. 5. SEM recordings of seeding particles (TiO_2) with four specifications. a D10;b D30;c D90;and d D30b.

3. Scattering characteristics of particles

3.1 Classification of scattering

Depending on the size of particles relative to the wavelength of incident light, there are simplifications which may be used to relate particle size to scattered intensity. The size parameter is defined by Eq.1:

$$\alpha = \pi d / \lambda \tag{1}$$

where α is a dimensionless parameter, d is the diameter of the scattering particle and λ is the wavelength of the light. There are three distinct scattering regimes, shown in Fig. 6, that α<<1 for Rayleigh Scattering, α~1 for Mie Scattering, α>>1for Mie Scattering [12].

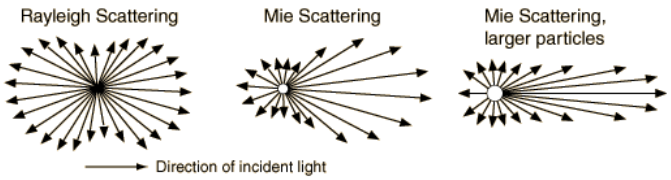

Fig. 6. Light scattering from spherical particles of different diameter [12].

3.2 Effect of scattering intensity [13]

For Rayleigh Scattering shown in Eq.2:

$$I = I_0 \frac{1+\cos^2\theta}{2R^2}\left(\frac{2\pi}{\lambda}\right)^4\left(\frac{n^2-1}{n^2+1}\right)^2\left(\frac{d}{2}\right)^6 \tag{2}$$

where I is scattered intensity, I_0 is incident intensity, θ is the scattering angle, R is the distance to the particle, λ is the wavelength of the light, n is the refractive index of the particle and d is actual diameter of the particle. For any given detector system and refractive index scattered intensity varies with d^6 in this regime.

For Mie Scattering, the relationship between particle diameter and scattered intensity in the regime is much more complicated than in either of the other regimes. The larger particles can be described using Eq.3:

$$I = I_0 K(n,\theta) d^2 \tag{3}$$

where I is scattered intensity, I_0 is incident intensity, K is a function of refractive index n and scattering angle θ, and d is actual particle diameter.

The variation of the scattering as a function of the ratio of $\alpha = \pi d / \lambda$ for the spherical particles with same refractive index n is shown in Fig. 7. It is very obvious that the scattering intensity increases with the increase in particle size in Rayleigh Scattering regime and the maximum value reach at point "A" around α=1 from the Fig.7. When α>1, the intensity varies in a way of damped oscillation. So the perfect particle size diameter $d = \alpha\lambda / \pi$ is around 200nm when the wavelength of the light is 532nm. Moreover, in PIV experiments light scattered at 90°from the incident light sheet is observed and strongly size dependent in the range of 0.001-0.1 for scattering in PIV. Furthermore refractive index of particles may be as large as possible.

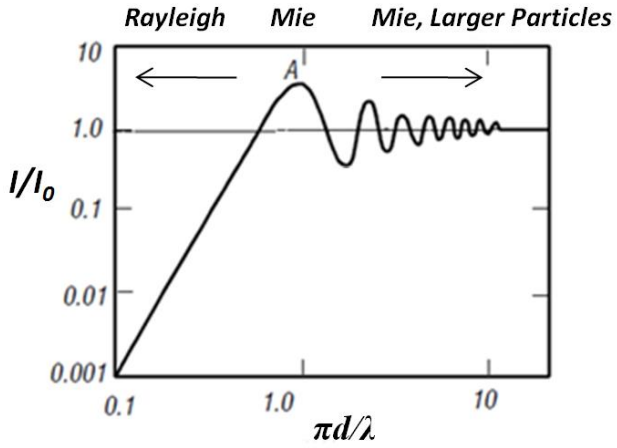

Fig. 7. Scattering intensity as a function of particle size (units of x, y-axis are non-dimensional) [14].

3.3 Experimental results

With the same light energy illuminations and seeding concentration, the amount of light scattered by D10, D30, D90 and D30b were assessed by inspecting the pixel intensity histograms using the same size interpretation area in the same locations shown in Fig. 8. The yellow square was considered as intercepted position before shock wave with a low particles concentration with 150pix×150pix. Four pictures shown in Fig. 9 were the intercepted results corresponded to four specifications of particles. In Fig. 10, the histograms of pixel intensity with different diameters were shown that although the four intercepted pictures have almost the same brightness, D90 has lower peak than D10, D30 and D30b, and the last three ones seem to have similar diameter due to approximative peaks and range of histograms agreed with the diameters estimation in Table 1.

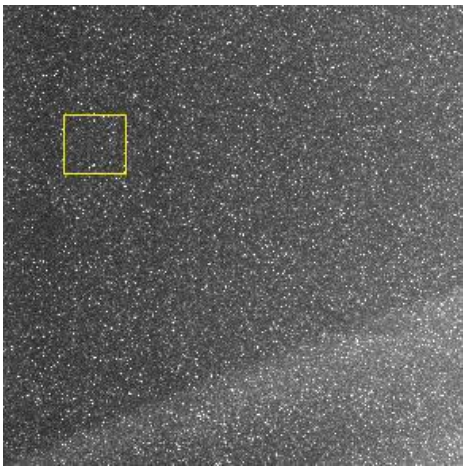

Fig. 8. The image of intercepted position.

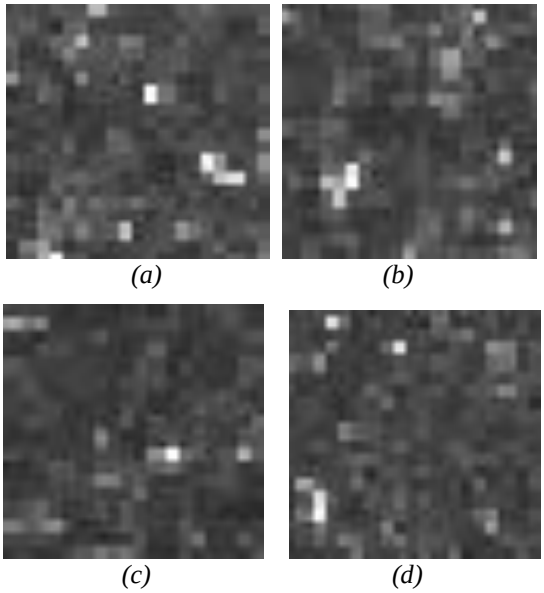

Fig. 9. The intercepted results with different diameters. (a) D10;(b) D30;(c) D90;and (d) D30b.

4. Tracking characteristics of particles

4.1 Theoretical analysis of the particle response

The application of PIV in a supersonic flow poses the restrictions on the spatial resolution due to the behavior of tracer particles in association with large velocity gradients.

To predict the particle behavior theoretically, a simplification of the equation of particle motion is used [14]. The relaxation time is given by Eq.4:

$$\tau = d_p^{\,2} \frac{\rho_p}{18\mu_f} \tag{4}$$

where ρ_p is the bulk density, 4230kg/m^3, d_p is the actual particles diameter and μ_f is the flow dynamic viscosity, 4.83×10^{-6}kg/(m·s). Next this equation will be used to estimate the actual particles.

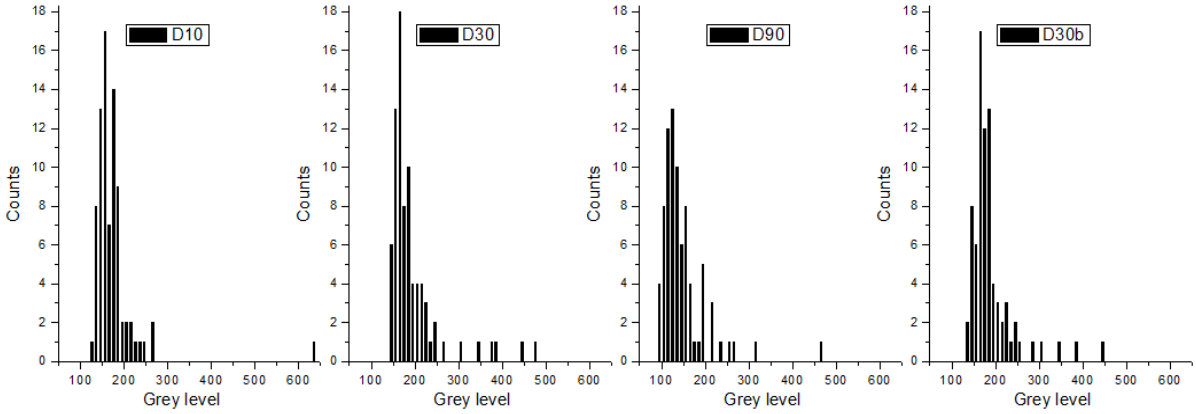

Fig. 10. Histograms of pixel intensity with different diameters (units of x,y-axis are equal to 1).

4.2 Measurements of the particles response

The fidelity of the trace particles was assessed by measuring the particle response across an oblique shock wave, which was generated by a 20° deflection damp at Ma=4.0. The velocity vector u which is extracted normal to shock wave from the results of PIV measurements (Fig. 11a) can be split into a normal component u_n, and a tangential component u_t with respect to the shock wave (Fig. 11b). The tangential component of the flow velocity is preserved across an oblique shock wave, and for the normal velocity component the relations for a normal shock can be applied. They show that the tangential velocity component remains unchanged across the shock wave as expected by theory and the normal velocity component is decelerated within a distance δ as the relaxation length shown in Table 2. The experimental relaxation length δ can be obtained in Fig. 8 which the value $\bar{y}$ is the distance from the wave ($\bar{y}$ is positive after wave and negative before wave). Therefore, the relaxation time τ can be obtained by $2\delta/(u_{n1}+u_{n2})$, among that $u_{n1}=340m/s$ and $u_2=120m/s$, u_{n1}, u_{n2} are the normal velocities before and after shock wave. Follow the Eq.4, the particle diameters can be estimated after the relaxation time τ to get. From the Table 2, consistency was found between the dynamic particle diameters and estimated particle diameters. Meanwhile, it is shown that the particle size was selected appropriately suitable. Therefore, smaller actual size of particles with diameter less than 200nm seems to be very difficult to obtained in the tests due to built-in agglomeration.

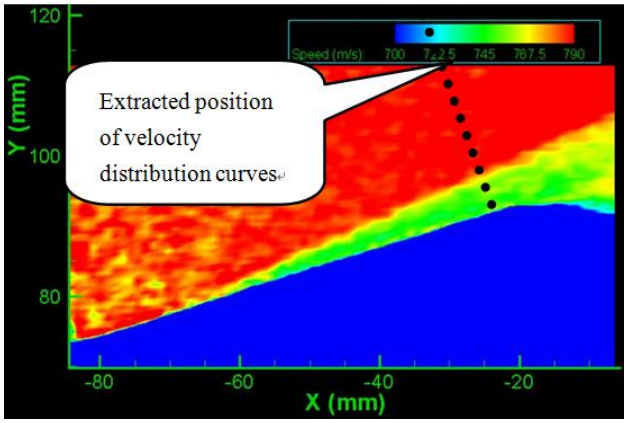

(a)

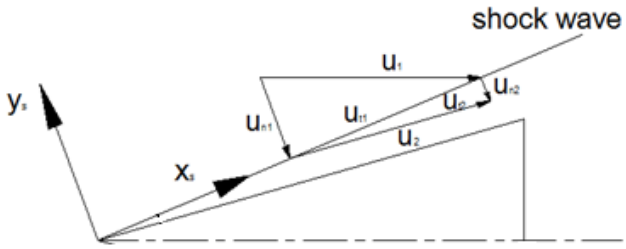

(b)

Fig. 11. (a) The Extracted position of velocity distribution curves; and (b) Oblique shock at a sharp cone; shock wave coordinate system(x_s-y_s).

5. Seeding techniques

The design of seeding generator for more homogenous distribution and less agglomeration of particles in the wind tunnel is crucial for PIV. Otherwise the safety of this facility requires proper material (stainless steel) and fasteners to withstand the intended pressure and heat. This seeding particles generator consists of three parts: the main vessel, top pipes and bottom pipe. Two holes on the vessel are connected to storage tube through top pipes and one bottom pipe regulated in large pressure range connects to the high pressure air supply. The accessories of the whole seeding system are shown in Fig. 13. During the test preparation, the supply of dry compressed air enters the seeding particles generator after pneumatic valve F2 opened. Then the seed particles mixed with compressed air are piped through high pressure pipe after the pneumatic valve F3 and F4 opened and injected into the free stream of wind tunnel. Due to reduce the turbulence of main flow mixed with particles in the test chamber, the seeding injection port is located in the upstream of the settling chamber and seemly far from the test chamber seen in Fig. 2.

Table 2. TiO_2 particles relaxation time in theory and experiments.

	Experimental relaxation length δ (mm)	Particles velocities across an oblique wave(m/s)	Experimental relaxation time τ [μs]	Estimated actual size[nm]	Experimental actual size[nm]
D10	0.7	230	3.04	200	249
D30	0.7	230	3.04	200	249
D90	1.1	230	4.78	300	282
D30b	0.7	230	3.04	200	249

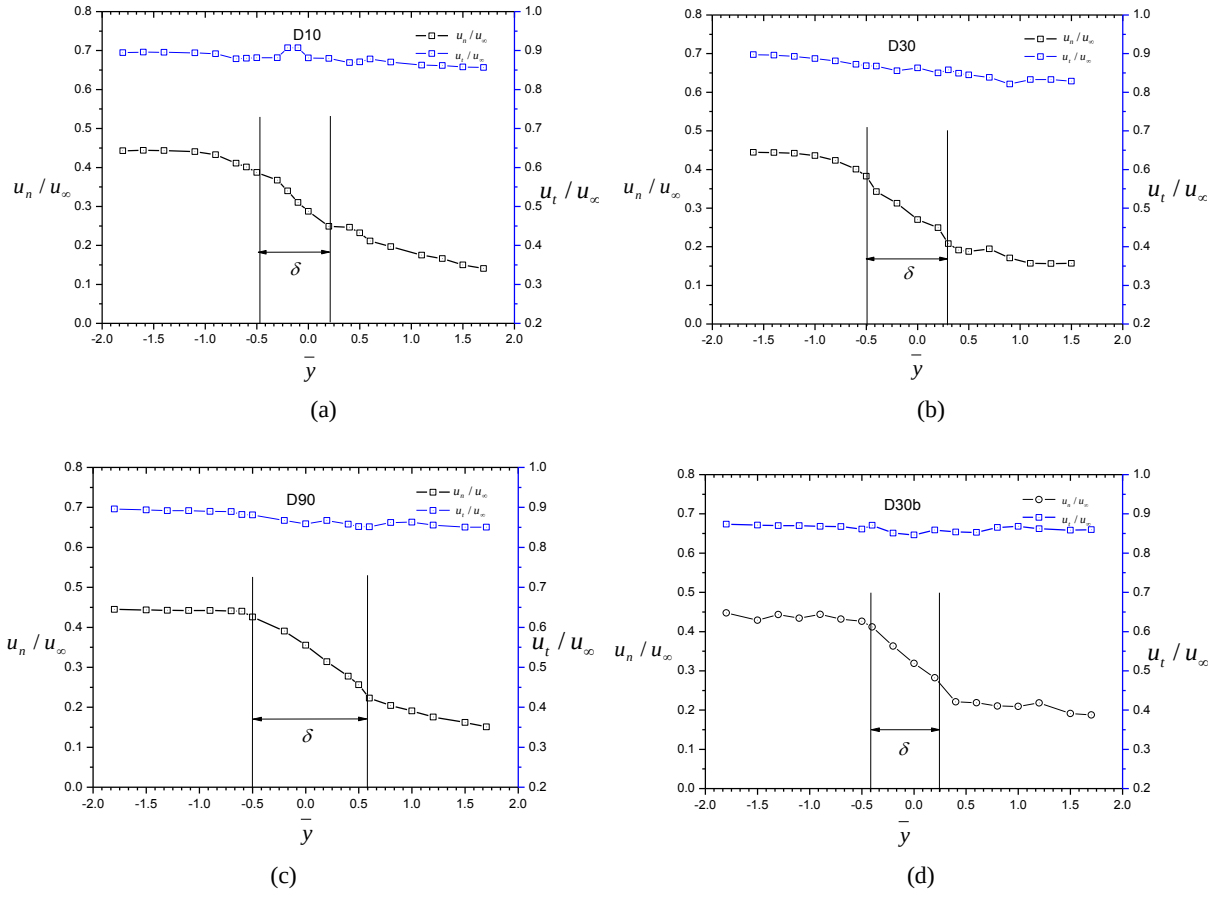

Fig. 12. Normal and tangential velocity lines with respect to the oblique shock with different diameters. (a) D10;(b) D30;(c) D90;and(d) D30b.

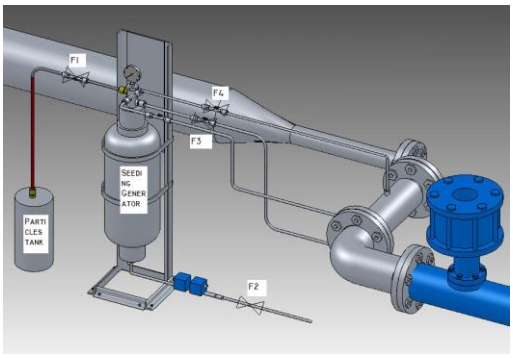

Fig. 13. Schematic sketch of seeding system.

The seeding concentration of TiO_2 was optimized by several preliminary experiments, and good results were obtained for a mass flow 0.02kg/s with the main flow 3kg/s, which corresponded to a seeding density of almost 100,000 particles/mm^3 in the test section at the time of capturing. More than 10 particles per interrogation window were satisfied the requirement of cross-correlation operation. Detailed design and operation of seeding system can be seen in a coming published paper 15. An origin picture of particles seeding over a damp model seems to be good shown in Fig. 14.

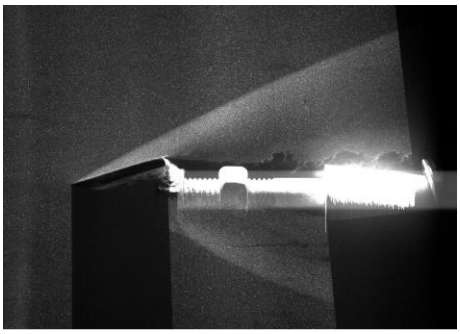

Fig. 14. Origin picture of particles seeding.

6. Results

6.1 Free stream flow assessment at Ma=4.0

As a basis of study, free stream flow assessment was presented firstly. The PIV measured results with different values of total temperature were shown in Table 3. The measured velocity results (averaged by 7 runs) were found to be less than 1% in defect with respect to those calculated by adiabatic flow theory.

The nozzle flow was measured by PIV at Ma=4.0 and T0=400K shown in Fig. 15. A field of view of about 100 ×180mm^2 parallel to the axis of symmetry. The spatial distribution of the free stream shows homogeneous in the center of nozzle flow. In the upper and lower parts, the flow velocity is lower and non-steady because the flow is under-expanded and slightly diverged at the nozzle tip.

Table 3. Comparison between the PIV measured free stream velocity and theoretical velocity.

Free stream velocity[m/s]					
	T0[K]	Theoretical velocity[m/s]	PIV measured velocity[m/s]	Difference measurement calculation [m/s]	Difference percent[%]
Ma=4.0	400	787.5	793	3.62	0.48
	350	677.6	684.1	6.5	0.96

6.2 Sharp cone flow at M=4.0

The flow over a sharp cone with a deflection angle of $\theta = 15°$ was measured by PIV and Schlieren. The PIV picture and schlieren visualization results were very much in accordance with each other and shown in Fig.16 (left). The shock wave angles inferred from schlieren and PIV picture were compared with the calculation by theory of perfect gas seen in Tab.4, where a good agreement was found. In Fig. 16 (right), the velocity distributions are more homogeneous at rear part and the position where the shock wave initialized at fore part is a little backward which ascribed to the effect of the surface reflection and the three-dimensional effect of model if the light sheet is not fully coincide with the bus bar of model.

Table 4. Shock wave angle comparison.

Ma	Shock wave angle[deg.]		
	Theory	Schlieren	PIV
4.0	21.71	21.9	21.6

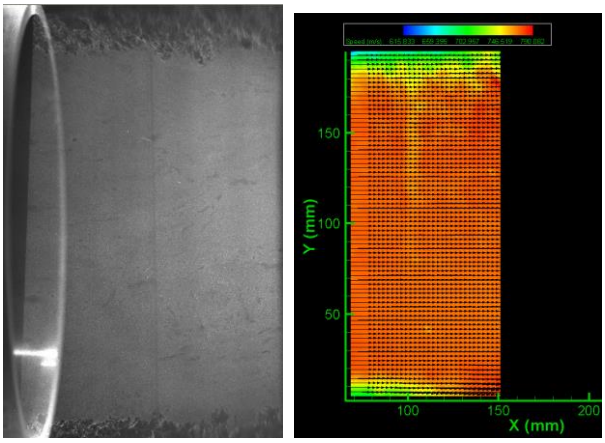

(a) *(b)*

Fig. 15. Mach 4.0 nozzle flow. (a) PIV picture with D30 and(b) Horizontal flow velocity.

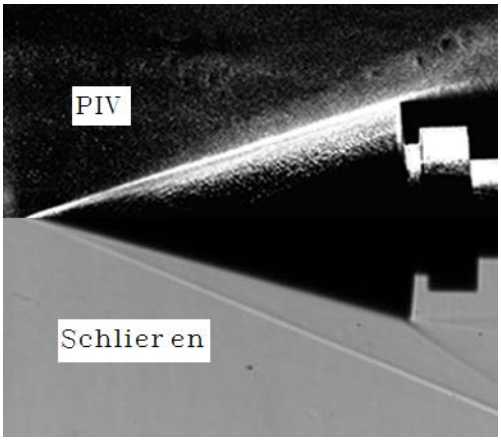

(a)

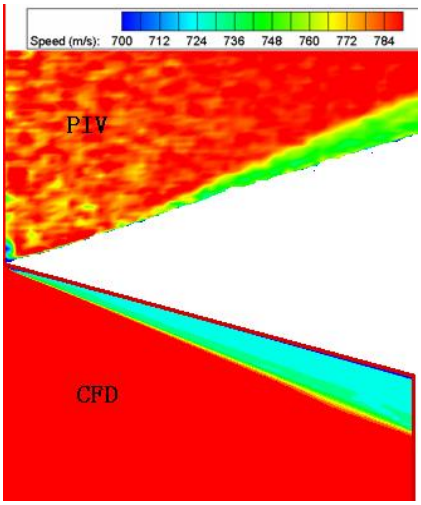

(b)

Fig. 16. (a) Comparison of PIV and Schlieren and (b) CFD results versus.

7. Conclusions

By analyzing the tracer particles scattering, tracking and seeding characteristics, TiO_2 particles with the dynamic diameter around 200nm is a kind of suitable particles for PIV measurements, and the particles are dispersed well by seeding particles generator. The velocities through the free stream are consistent with the values theoretically designed very well, and the flow across the shocks regions are in accordance with CFD and schlieren visualization with little bias error. With the current research results, it can be seen that with appropriate seeding techniques, the PIV technique could be an effective approach to the supersonic flow as well as for subsonic flow regimes.

References

[1] L. M. Lourengo, in M. L. Riethmuller (Ed.), Particle Image Velocimetry, VKI Lecture Series 1996-03, 1996.
[2] F. Scarano, Particle Image Velocimetry, Topics Appl. Physics **112**, 445 (2008).
[3] W. M. Humphreys, S. M. Bartram, J. L. Blackshire, AIAA Paper 93-0411, Jan. 1993.
[4] C. S. Moraitis, M. L. Riethmuller, Proc. 4th Int. Symp. Appl. of Laser Anemometry to Fluid Dyn, 1988.
[5] J. Kompenhans, R. Hocker, M. L. Riethmuller, (Eds.): Particle image displacement velocimetry, VKI Lecture Series, 1988.
[6] A. Melling, Measurement Science and Technology. **8**, 1406 (1997).
[7] F. F. J. Schrijer, F. Scarano, B. W. Oudheusden, AIAA paper 2005-3331, 2005.
[8] D. Ragni, F. F. J. Schrijer, B. W. Oudheusden, F. Scarano, Experiments in Fluids, **50**(1), 53 (2010).
[9] S. H. Yi, Z. X. Hou, C. R. Wang, Experiments and Measurements in Fluid Mechanics, **7**(2), 59 (2003).
[10] Y. X. Zhao, S. H. Yi, et al., Journal of National University of Defense Technology, **29**(1), 12 (2007).
[11] Q. Dai, et al., Journal of Beijing University of Aeronautics and Astronautics, **27**(6), 666 (2001).
[12] Max Born, Emil Wolf, Cambridge University Press. 2001.
[13] Electronic warfare and radar systems engineering handbook, NAWCWPNS TP-8347, 1997.
[14] Z. Zhang, Chapter 7 of LDA Application Methods, Experimental Fluid Mechanics, 2010.
[15] Z. Rong, F. Chen, H. Liu, Journal of Experiments in Fluid Mechanics, **6**(6), **53** (2012).

*Corresponding author: zhang_baogu@126.com